A finite element scheme to study the nonlinear optical response of a finite grating without and with defect

A. Suryanto*† E. van Groesen, M. Hammer and H.J.W.M. Hoekstra
MESA$^+$ Research Institute, University of Twente, The Netherlands

September 25, 2002

Abstract

We present a simple numerical scheme based on the Finite Element Method (FEM) using transparent-influx boundary conditions to study the nonlinear optical response of a finite one-dimensional grating with Kerr medium. Restricting first to the linear case, we improve the standard FEM to get a fourth order accurate scheme maintaining a symmetric-tridiagonal structure of the finite element matrix. For the full nonlinear equation, we implement the improved FEM for the linear part and a standard FEM for the nonlinear part. The resulting nonlinear system of equations is solved using a weighted-averaged fixed-point iterative method combined with a continuation method. To illustrate the method, we study a periodic structure without and with defect and show that the method has no problem with large nonlinear effect. The method is also found to be able to show the optical bistability behavior of the ideal and the defect structure as a function of both the frequency or the intensity of the input light. The bistability of the ideal periodic structure can be obtained by tuning the frequency to a value close to the bottom or top linear band-edge while that of the defect structure can be produced using a frequency near the defect mode or near the bottom of the linear band-edge. The threshold value can be reduced by increasing the number of layer periods. We found that the threshold needed for the defect structure is much lower then that for a strictly periodic structure of the same length.

Key words: finite element method, optical bistability, periodic (defect) structure, transparent-influx boundary condition

1 Introduction

The propagation of waves through periodic structures has been extensively studied in recent years, see e.g. Soukoulis (1993 and 1996). An essential property of these structures is the existence of a frequency band gap in which propagating modes are absent. When a Kerr nonlinearity is introduced it can effect many interesting phenomena such as optical switching which is caused by a dynamic shifting of the band-edge, see e.g. Tran (1996 and 1997) and Wang et al. (1997). In Tran (1996) the author introduced an optical switch in a nonlinear finite grating using two light pulses at different frequencies, a probe beam near the band-edge and a strong pump beam in the middle of the band gap to alter the index of refraction of the structure. The pump beam is used to control the position of the band-edge of the structure so as to transmit or reflect the probe beam. A drawback of this procedure was that the pump beam did not penetrate far into the structure and therefore did not change the effective index of refraction significantly. To increase the field penetration but not to transmit, Tran (1997) have introduced a defect layer in the

*This research is supported by the Technology Foundation STW (TWI. 4813), applied science division of NWO and the technology programme of the Ministry of Economic Affairs, The Netherlands

†Applied Mathematics, University of Twente, P.O. Box 217, 7500 AE Enschede, The Netherlands; on leave from Jurusan Matematika, Universitas Brawijaya, Jl. MT Haryono 167 Malang, Indonesia; email:A.Suryanto@math.utwente.nl

grating structure and shown that the defect structure can indeed improve the performance of these switching devices. Since the switching mechanism consists of two pulses at difference frequencies, Tran (1996 and 1997) used the nonlinear finite difference time domain (NFDTD) method to go beyond the slowly varying envelope approximation and to avoid the complexity of the problem due to the interaction between two frequencies.

A different approach for an all-optical switch is based on the self-switching arrangement where the output is dependent on some characteristics of the input light, e.g. power. An example is optical bistability which can be realized in a nonlinear periodic structure. In this case the input light is monochromatic. While the threshold value of bistability needed by a periodic structure is relatively high, He and Cada (1991) proposed a combined structure which is composed of a distributed feedback structure and a phase-matching layer placed in a Fabry-Perot cavity where the threshold is significantly reduced. Recently, Lidorikis et al. (1997) and Wang et al. (1997) found that when a single nonlinear defect layer is introduced into a linear periodic structure then the threshold value of the bistability is compatible with that of the structure proposed by He and Cada (1991). Throughout this paper we study a bistability that uses a monochromatic light input in finite periodic structures without and with a defect. For the defect structure, the nonlinearity will not only be introduced in the defect layer but also in the higher and/or lower index layers. Because we deal with a single frequency, the Maxwell's equations are reduced to a nonlinear Helmholtz equation which is simpler. Furthermore, the numerical calculations in frequency domain are generally more efficient than those in time domain.

Since 30 years ago, a lot of efforts have been devoted to study the phenomenon of bistability in a periodic structure. A number of authors, e.g. Marburger and Felber (1978), Winful *et al.* (1979), Danckaert *et al.* (1989 and 1991) proposed an analytical formalism for this problem. All these formalisms are derived within three basic approximations, i.e. the slowly varying envelope approximation (SVEA), the approximation of nonlinear terms that appear in the interface conditions and the omission of spatial third harmonics generated in the structure. Treatments that make use of the full nonlinear interface conditions in the nonlinear transfer matrix were given by Agarwal and Dutta Gupta (1987) and Dutta Gupta and Agarwal (1987).

Another approach to solve the nonlinear wave equation was proposed by Chen and Mills (1987a, 1987b). In this approach the nonlinear Helmholtz is transformed into a phase-amplitude equation. By combining with energy conservation the phase-amplitude equation is written in integral form. The integral equation together with the continuity conditions at the interfaces are solved numerically. Recently this method has been implemented by Lidorikis *et al.* (1997) to investigate the localized mode solution for a single nonlinear layer sandwiched between two linear periodic structures. The authors show that the structure exhibits bistability via a defect mode.

A semi-analytic method has been proposed by Wang *et al.* (1997) to study the optical bistability in a linear periodic structure with a single nonlinear defect layer in the center. The transfer matrix method is used for the linear part and a finite difference method is implemented for the nonlinear layer. The left and right linear parts and the nonlinear layer are linked using appropriate interface conditions. They found that the threshold of bistability for the defect structure is much lower than that for the corresponding periodic structure.

In this paper we apply a finite element method (FEM) together with transparent-influx boundary conditions to study the nonlinear optical response of a finite periodic structure without and with defect. In Sec. 2 we derive the 1D nonlinear Helmholtz equation including transparent-influx boundary conditions. Then this equation is transformed into a variational numerical scheme in Sec. 3. For the linear scheme we improve the standard FEM to get a fourth order accurate scheme that maintains the symmetric-tridiagonal structure of the finite element matrix. For the full nonlinear equation, we implement the improved FE scheme for the linear part and a standard FEM for the nonlinear part. Then we obtain a nonlinear system of equations that will be solved using a weighted-averaged fixed-point iterative method combined with a continuation method. Recently similar combination has been used by Lu *et al.* (1998) to solve a nonlinear equation obtained from the nonlinear transfer matrix formalism. In Sec. 4 we apply our numerical scheme to study the optical bistability in a finite ideal periodic structure and in a finite grating with a defect layer. Conclusions and remarks will be given in the last section.

2 Wave equation and its boundary conditions

We consider the propagation of optical electromagnetic field through one-dimensional, periodic, dispersionless and lossless stratified dielectric media with a Kerr nonlinearity. The electric and the magnetic fields have the form,

$$\mathbf{E}(z,t) = [0, E_y(z,t), 0], \tag{1}$$
$$\mathbf{H}(z,t) = [H_x(z,t), 0, 0]. \tag{2}$$

Assuming that the media are isotropic, the polarization $\mathbf{P}$ is parallel to $\mathbf{E}$:

$$\mathbf{P}(z,t) = [0, P_y(z,t), 0]. \tag{3}$$

Maxwell's equations then reduce to the wave equation

$$\frac{\partial^2 E_y(z,t)}{\partial z^2} - \frac{1}{c^2}\frac{\partial^2 E_y(z,t)}{\partial t^2} = \mu_0 \frac{\partial^2 P_y(z,t)}{\partial t^2}. \tag{4}$$

For a material with a Kerr nonlinearity, the polarization P_y is given by (see He and Liu, 1999)

$$P_y(z,t) = \varepsilon_0 \left\{ \chi^{(1)}(z) E_y(z,t) + \chi^{(3)}(z) |E_y(z,t)|^2 E_y(z,t) \right\}, \tag{5}$$

where $1 + \chi^{(1)}(z) \equiv \epsilon_r(z) \equiv n^2(z)$ describes the linear dielectric constant, n is the refractive index and $\chi^{(3)}$ is the third-order nonlinear susceptibility. If excited by an input beam with a single frequency ω, the polarization (5) does not lead to the generation of high order harmonics in the Kerr medium. Hence we can look for stationary solutions of the form

$$E_y(z,t) = e^{i\omega t} u(z). \tag{6}$$

The harmonic time dependence leads to the scalar nonlinear Helmholtz equation (NLH)

$$\frac{d^2 u(z)}{dz^2} + k^2 \left(n^2(z) + \chi^{(3)}(z) |u(z)|^2 \right) u(z) = 0, \tag{7}$$

where $k^2 = \omega^2/c^2$ with $c^2 = \frac{1}{\varepsilon_0 \mu_0}$ is the speed of light. Notice that equation (7) holds for arbitrary $n(z)$ and $\chi^{(3)}(z)$. In many applications, we deal with the NLH (7) in the presence of an incident wave from either a linear or nonlinear homogeneous medium to a scattering structure (e.g. the linear or nonlinear periodic structure) that is followed with a linear or nonlinear homogeneous region. Here we assume that the medium outside the scattering structure is linear and homogeneous with refractive index n_0. In order to solve this problem numerically, we have to limit the original unbounded domain to a finite computational domain. In doing so, we have to provide boundary conditions that can transmit completely the incident wave and simultaneously be transparent for all outgoing waves. These boundary conditions are called transparent-influx boundary conditions (TIBC). Such boundary conditions will be derived as follows. Outside the scattering structure, the Helmholtz equation is linear and has a constant refractive index n_0. Therefore this equation can be factorized as

$$\left(\frac{d}{dz} - ikn_0 \right) \left(\frac{d}{dz} + ikn_0 \right) u = 0, \tag{8}$$

yielding the following boundary conditions:

$$\frac{du}{dz} - ikn_0 u = -2ikn_0 A, \quad z = 0 \tag{9}$$
$$\frac{du}{dz} + ikn_0 u = 0, \qquad z = z_{\max}. \tag{10}$$

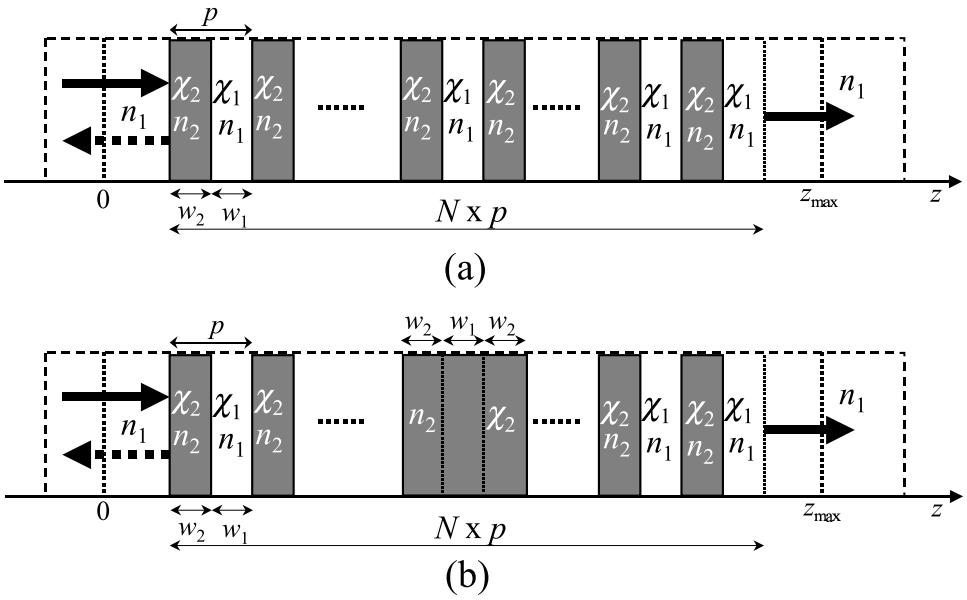

Figure 1: Schematic view of two structures considered in this paper. (a) Periodic structure that consists of N alternating layers. (b) For the defect structure, the center layer with original refractive index n_1 and nonlinearity χ_1 is replaced by another layer of index n_2 and nonlinearity χ_2.

The first boundary condition (9) is an influx condition for an incident wave with wavenumber k and constant amplitude A and is simultaneously transparent for the back scattered field. The second condition (10) is a transparent boundary condition for the right-travelling wave.

Fig. 1 sketches the two grating structures analyzed in this paper. The periodic structure is a structure which has $2N+1$ alternating layers of lower index n_1 and higher index n_2. For the defect structure, the center layer with original refractive index n_1 is replaced by another layer of index n_2. Such a defect structure may be viewed as two separated multilayer mirrors enclosing the defect layer and thus it can be considered as a Fabry-Perot cavity (see e.g. Kasyap 1999 and Bayindir *et al.* 2001). Notice that the refractive index of the linear medium outside the scattering structure is chosen to be n_1. For the sake of simplicity we normalize the position and frequency variables to a reference wavelength λ_0 : $\zeta = z/\lambda_0, \widetilde{\omega} = \omega\lambda_0/c$; and the wave amplitude to the incoming wave amplitude: $U = u/A$. Now the NLH and the boundary conditions read

$$\begin{aligned} \frac{d^2U(\zeta)}{d\zeta^2} + \widetilde{\omega}^2\left(n^2(\zeta) + \gamma(\zeta)\left|U(\zeta)\right|^2\right)U(\zeta) = 0, & \\ \frac{dU(\zeta)}{d\zeta} - i\widetilde{\omega}n_0U(\zeta) = -2i\widetilde{\omega}n_0, \qquad & \zeta = 0 \\ \frac{dU(\zeta)}{d\zeta} + i\widetilde{\omega}n_0U(\zeta) = 0, \qquad & \zeta = \zeta_{\max}, \end{aligned} \tag{11}$$

where $\gamma = A^2\chi$. Hence, γ can be considered alternatively as input intensity or strength of the nonlinearity.

3 Numerical method

3.1 Linear scheme

In this section we discuss a numerical method to solve equation (11) based on a variational method. We first concentrate to the linear Helmholtz equation where $\gamma = 0$ and consider the functional

$$F_L(U) = -\frac{1}{2}\int_{-\infty}^{\infty}\left[\left|\frac{dU}{d\zeta}\right|^2 - \widetilde{\omega}^2 n^2 |U|^2\right] d\zeta \tag{12}$$

which can also be written as

$$F_L(U) = F_1(U) + F_2(U) + F_3(U) \tag{13}$$

where

$$F_1(U) = -\frac{1}{2}\int_{-\infty}^{0}\left[\left|\frac{dU}{d\zeta}\right|^2 - \widetilde{\omega}^2 n^2 |U|^2\right] d\zeta,$$
$$F_2(U) = -\frac{1}{2}\int_{0}^{\zeta_{\max}}\left[\left|\frac{dU}{d\zeta}\right|^2 - \widetilde{\omega}^2 n^2 |U|^2\right] d\zeta,$$
$$F_2(U) = -\frac{1}{2}\int_{\zeta_{\max}}^{\infty}\left[\left|\frac{dU}{d\zeta}\right|^2 - \widetilde{\omega}^2 n^2 |U|^2\right] d\zeta.$$

As it is assumed that the medium outside the grating structure is linear homogeneous with refractive index n_0, without loss of generality, the solution of the linear part of equation (11) can be written as

$$U(\zeta) = \begin{cases} \exp(-i\widetilde{\omega} n_0 \zeta) + r\exp(i\widetilde{\omega} n_0 \zeta) & , \zeta \le 0; \\ U(\zeta) & , \zeta \in [0, \zeta_{\max}]; \\ t\exp(-i\widetilde{\omega} n_0 \zeta) & , \zeta \ge \zeta_{\max}. \end{cases} \tag{14}$$

By substituting (14) into the functional (13), one can show that if the variational derivative of this functional vanishes, $\delta_U F_L = 0$, then the field $U(\zeta)$ satisfies the linear part of NLH (11).

Let us assume that the interval $[0, \zeta_{\max}]$ is divided into M subintervals of equal length $h = \zeta_{\max}/M$ by choosing the nodal points $\zeta_j = jh$ for $j = 0 \ldots M$. Now we approximate the function $U(\zeta)$ as a linear combination of a basis $\{\varphi_m(\zeta)\}_0^M$:

$$U(\zeta) \cong \sum_{j=0}^{M} \widehat{U}_j \varphi_j(\zeta). \tag{15}$$

Here we define the base functions φ_m by piecewise linear interpolation ("tent" function) between the nodal values $\varphi_m(\zeta_j)$, which are

$$\varphi_m(\zeta_j) = \delta_{m,j}, \quad m, j = 0, 1, \ldots, M. \tag{16}$$

Then $\widehat{U}_m$ is the approximation of $U(\zeta)$ at $\zeta = \zeta_m$. Using (15), the functional F_2 can be approximated by a function $\widetilde{F_2}$ such that $F_2(U) \cong \widetilde{F_2}\left(\widehat{U}\right)$ where $\widehat{U} = \left(\begin{array}{cccc} \widehat{U}_0, & \widehat{U}_1, & \cdots, & \widehat{U}_M \end{array}\right)^T$. The condition $\delta_U F_L = 0$ therefore corresponds to

$$\delta_U F_1 + \nabla\widetilde{F_2}\left(\widehat{U}\right) + \delta_U F_3 = 0 \tag{17}$$

where

$$\delta_U F_1 = -i\widetilde{\omega} n(0) U(0) + 2i\widetilde{\omega} n(0)$$
$$\delta_U F_2 = -i\widetilde{\omega} n(\zeta_{\max}) U(\zeta_{\max}) \tag{18}$$

which leads to a linear system (by assuming that each discontinuity of the structure coincides with a grid point)

$$\left(\frac{1}{h}P+\frac{1}{6}h\widetilde{\omega}^2Q\right)\widehat{U}=v \tag{19}$$

where

$$P=\begin{pmatrix} -1-ih\widetilde{\omega}\widehat{n}_0 & 1 & 0 & . & . & 0 \\ 1 & -2 & 1 & 0 & . & . \\ 0 & . & . & . & . & 0 \\ . & . & 0 & 1 & -2 & 1 \\ 0 & . & . & 0 & 1 & -1-ih\widetilde{\omega}\widehat{n}_M \end{pmatrix},$$

$$Q=\begin{pmatrix} 2\widehat{n}_0^2 & \widehat{n}_0^2 & 0 & . & . & 0 \\ \widehat{n}_0^2 & 2\left(\widehat{n}_0^2+\widehat{n}_1^2\right) & \widehat{n}_1^2 & 0 & . & . \\ 0 & . & . & . & . & 0 \\ . & . & 0 & \widehat{n}_{M-2}^2 & 2\left(\widehat{n}_{M-2}^2+\widehat{n}_{M-1}^2\right) & \widehat{n}_{M-1}^2 \\ 0 & . & . & 0 & \widehat{n}_{M-1}^2 & 2\widehat{n}_{M-1}^2 \end{pmatrix},$$

and $v=\begin{pmatrix} -2i\widetilde{\omega}\widehat{n}_0 & 0 & ... & 0 \end{pmatrix}^T$ and $\widehat{n}_j$ is the linear index in the interval (ζ_j,ζ_{j+1}). In the following this scheme is called the standard finite element method (FEM).

We will examine the order of accuracy of the numerical scheme (19). For uniform medium with index n, the j-th equation of (19) can be written as

$$\delta_\zeta^2\widehat{U}_j+\frac{1}{6}\widetilde{\omega}^2\widehat{n}^2\left(\widehat{U}_{j-1}+4\widehat{U}_j+\widehat{U}_{j+1}\right)=0, \tag{20}$$

where

$$\delta_\zeta^2\widehat{U}_j=\frac{1}{h^2}\left(\widehat{U}_{j+1}-2\widehat{U}_j+\widehat{U}_{j-1}\right). \tag{21}$$

Using a Taylor expansion, it can be shown that

$$\frac{d^2U\left(\zeta_j\right)}{d\zeta^2}=\delta_\zeta^2\widehat{U}_j-\frac{h^2}{12}\frac{d^4U\left(\zeta_j\right)}{d\zeta^4}+O\left(h^4\right) \tag{22}$$

$$\frac{d^2U\left(\zeta_j\right)}{d\zeta^2}+\widetilde{\omega}^2\widehat{n}^2U\left(\zeta_j\right)=\delta_\zeta^2\widehat{U}_j+\frac{1}{6}\widetilde{\omega}^2\widehat{n}^2\left(\widehat{U}_{j-1}+4\widehat{U}_j+\widehat{U}_{j+1}\right)+\text{Res}, \tag{23}$$

where $\text{Res}=-\frac{1}{12}\widetilde{\omega}^2\widehat{n}^2h^2\frac{d^2U(\zeta_j)}{d\zeta^2}+O\left(h^4\right)$. This shows that the standard scheme (19) for the interior points is only second order accurate. The accuracy of the standard discrete boundary conditions can be checked as follows. First we discretized the TIBC at $\zeta=0$ (11) using a central difference:

$$\frac{1}{2h}\left(\widehat{U}_1-\widehat{U}_{-1}\right)-i\widetilde{\omega}\widehat{n}_0\widehat{U}_0=-2i\widetilde{\omega}\widehat{n}_0, \tag{24}$$

which is an $O\left(h^2\right)$ approximation. Then this approximation is used to eliminate the term $\widehat{U}_{-1}$ in (23) with $j=0$ to recover the standard FEM at the left boundary (and similarly for the right boundary). Because both (23) and (24) are of $O\left(h^2\right)$, the usual FEM at the boundaries is also $O\left(h^2\right)$.

Now we wish to improved the order of accuracy of the standard scheme (19). By applying the central difference to the first term of Res and adding it to (23) we obtain a fourth-order scheme

$$\frac{d^2U\left(\zeta_j\right)}{d\zeta^2}+\widetilde{\omega}^2\widehat{n}^2U\left(\zeta_j\right)=\left(1-\frac{1}{12}\widetilde{\omega}^2\widehat{n}^2h^2\right)\delta_\zeta^2\widehat{U}_j+\frac{1}{6}\widetilde{\omega}^2\widehat{n}^2\left(\widehat{U}_{j-1}+4\widehat{U}_j+\widehat{U}_{j+1}\right)+O\left(h^4\right) \tag{25}$$

which leads to a linear system of equations (after modifying the boundary condition in a similar way):

$$\left(\frac{1}{h}P_1+\frac{1}{6}h\widetilde{\omega}^2Q\right)\widehat{U}=v_1 \tag{26}$$

where

$$P_1 = \begin{pmatrix} -\alpha_0\left(1+ih\widetilde{\omega}\widehat{n}_0\right) & \alpha_0 & 0 & . & . & 0 \\ \alpha_0 & -\left(\alpha_0+\alpha_1\right) & \alpha_1 & 0 & . & . \\ 0 & . & . & . & . & 0 \\ . & . & 0 & \alpha_{M-2} & -\left(\alpha_{M-2}+\alpha_{M-1}\right) & \alpha_{M-1} \\ 0 & . & . & 0 & \alpha_{M-1} & -\alpha_{M-1}\left(1+ih\widetilde{\omega}\widehat{n}_M\right) \end{pmatrix},$$

with $\alpha_j = 1 - \frac{1}{12}\widetilde{\omega}^2\widehat{n}_j^2h^2$ and $v_1 = \begin{pmatrix} -(1+k^2h^2/12)2i\widetilde{\omega}\widehat{n}_0 & 0 & \ldots & 0 \end{pmatrix}^T$. Notice that the resulting matrix is still tridiagonal and symmetric. This fourth-order scheme is called improved FEM.

Based on our numerical experiments we found that the numerical amplitude and phase error of the standard FEM is of $O\left(h^2\right)$. When we apply the improved FEM (26) to both a uniform structure and a periodic structure with $N = 2$ and $N = 20$, the numerical results show that the numerical error is indeed $O\left(h^4\right)$, as expected.

3.2 Nonlinear scheme

In the previous section we have discussed a numerical method to solve the linear Helmholtz equation. Here we consider the complete NLH (11). The numerical method is basically the same as for the linear case but with an additional nonlinear term $\widetilde{\omega}^2\gamma\left(\zeta\right)\left|U\left(\zeta\right)\right|^2U\left(\zeta\right)$. The functional (12) has to be extended with

$$F_{NL}\left(U\right) = \frac{1}{4}\int_0^{\zeta_{\max}} \widetilde{\omega}^2\gamma\left(\zeta\right)\left|U\right|^4 d\zeta. \tag{27}$$

As in the previous section, we approximate the additional contribution F_{NL} as follows

$$\begin{aligned} F_{NL}\left(U\right) &\cong \widetilde{F_{NL}}\left(\widehat{U}\right) \\ &= \frac{h}{20}\widetilde{\omega}^2\sum_{j=0}^{M-1}\widehat{\gamma}_j\widetilde{F_{NL}}_j \end{aligned} \tag{28}$$

where $\widehat{\gamma}_j$ is the nonlinear coefficient in the interval (ζ_j, ζ_{j+1}),

$$\begin{aligned} \widetilde{F_{NL}}_j\left(\widehat{U}\right) = &\left|\widehat{U}_j\right|^4 + \frac{1}{2}\left|\widehat{U}_j\right|^2\left(\widehat{U}_j\widehat{U}_{j+1}^* + \widehat{U}_j^*\widehat{U}_{j+1}\right) + \frac{1}{3}\left|\widehat{U}_j\right|^2\left|\widehat{U}_{j+1}\right|^2 \\ &+ \frac{1}{6}\left(\widehat{U}_j^2\widehat{U}_{j+1}^{*2} + 2\left|\widehat{U}_j\right|^2\left|\widehat{U}_{j+1}\right|^2 + \widehat{U}_j^{*2}\widehat{U}_{j+1}^2\right) \\ &+ \frac{1}{2}\left|\widehat{U}_{j+1}\right|^2\left(\widehat{U}_j\widehat{U}_{j+1}^* + \widehat{U}_j^*\widehat{U}_{j+1}\right) + \left|\widehat{U}_{j+1}\right|^4, \end{aligned} \tag{29}$$

and U^* is the conjugate of U. The partial derivatives of $\widetilde{F_{NL}}\left(\widehat{U}\right)$ are

$$\begin{aligned} \frac{\partial\widetilde{F_{NL}}}{\partial\widehat{U}_j} = &\mu_{j-1}\left(\frac{2}{3}\widehat{U}_{j-1}\widehat{U}_j^* + \left|\widehat{U}_{j-1}\right|^2 + 2\left|\widehat{U}_j\right|^2\right)\widehat{U}_{j-1} \\ &+ \mu_{j-1}\left(\widehat{U}_j\widehat{U}_{j-1}^* + \frac{4}{3}\left|\widehat{U}_{j-1}\right|^2 + 4\left|\widehat{U}_j\right|^2\right)\widehat{U}_j \\ &+ \mu_j\left(\widehat{U}_j\widehat{U}_{j+1}^* + \frac{4}{3}\left|\widehat{U}_{j+1}\right|^2 + 4\left|\widehat{U}_j\right|^2\right)\widehat{U}_j \\ &+ \mu_j\left(\frac{2}{3}\widehat{U}_{j+1}\widehat{U}_j^* + \left|\widehat{U}_{j+1}\right|^2 + 2\left|\widehat{U}_j\right|^2\right)\widehat{U}_{j+1}, \end{aligned} \tag{30}$$

where $\mu_j = \frac{h}{20}\widetilde{\omega}^2\widehat{\gamma}_j$. Adding the nonlinear term (30) to the linear scheme (26), we obtain:

$$\left(\frac{1}{h}P_1 + \frac{1}{6}h\widetilde{\omega}^2 Q + R\left(\widehat{U}\right)\right)\widehat{U} = v, \tag{31}$$

where $\widetilde{\nabla F_{NL}}\left(\widehat{U}\right) = R\left(\widehat{U}\right)\cdot\widehat{U}$. Equation (31) is a system of nonlinear equations that is usually solved using a fixed-point iterative method (see e.g. Atkinson, 1989):

$$\left(\frac{1}{h}P_1 + \frac{1}{6}h\widetilde{\omega}^2 Q + R\left(\widehat{U}^{(m)}\right)\right)\widehat{U}^{(m+1)} = v, \tag{32}$$

where $m = 1, 2, 3...$ is the iteration step with $\widehat{U}^{(1)}$ is taken from the solution of the linear problem. The iteration process is stopped when

$$\left\|\widehat{U}^{(m+1)} - \widehat{U}^{(m)}\right\| < \varepsilon \tag{33}$$

for small ε.

In general the fixed-point iterative algorithm leads to a convergent solution when there exist a unique solution. However, in the case of bistability where the solution is not unique, this iterative method may not be converging. As an example, we show in Fig. 2 the transmissivity $|T|^2 = \left|\widehat{U}_M\right|^2$ of a defect layer with $N = 10$; $\gamma_1 = 0$; $\gamma_2 = 10^{-2}$ and $\widetilde{\omega} = 3.8483$ as a function of the iteration number. The dotted line is calculated using the fixed-point iterative method that gives a non-convergent solution. In order to take care of the divergence problem in the fixed-point iterative method, we replace the argument of R in (32) with the weighted averages of $\widehat{U}^{(m-1)}$ and $\widehat{U}^{(m)}$ such that

$$\left(\frac{1}{h}P_1 + \frac{1}{6}h\widetilde{\omega}^2 Q + R\left(\widehat{U}^{(m-1/2)}\right)\right)\widehat{U}^{(m+1)} = v, \tag{34}$$

where $\widehat{U}^{(m-1/2)} = \sigma\widehat{U}^{(m)} + (1-\sigma)\widehat{U}^{(m-1)}$with σ, satisfying $0 < \sigma \leq 1$, is a parameter used to control the weight of $\widehat{U}^{(m)}$. Since $\widehat{U}^{(m-1/2)}$ is between $\widehat{U}^{(m)}$ and $\widehat{U}^{(m-1)}$, if the series $\widehat{U}^{(m)}$ is convergent then the series $\widehat{U}^{(m-1/2)}$ is also convergent; and furthermore both of those series have the same limit. Based on our numerical experiments, the iterative method (34) produces convergent solutions for sufficiently small values of σ. However the smaller σ needs a larger number of iterations. As an example, we plot in Fig. 2 the transmissivity of a defect structure as a function of the iteration number for $\sigma = 1, 1/3$, and $1/10$, respectively. Practically we first choose $\sigma = 1$. If it does not converge, we take a smaller value of σ. For the calculations in this paper we set the tolerance $\varepsilon = 10^{-6}$ and it is found that the iteration procedure (34) is always converging for $\sigma = 1/3$.

We notice that the iterative method (34) is only converging to one solution, whereas in the case of bistability there are two stable solutions, Therefore we still need to find another solution besides the one obtained from (34). Considering the nature of bistability, i.e. the transmissivity depends not only on the input intensity alone but also on the history of it, Lu *et al.* (1998) suggest to include the history of the input intensity in the calculation. In our case, we start by solving (34) for a nonlinearity value $\gamma^{(0)}$ that is relatively far from the bistability using the linear solution as an initial guess $\widehat{U}^{(1)}$. Then we use the solution of this calculation as a starting point for $\gamma^{(1)} > \gamma^{(0)}$ and so on. In this algorithm, when the nonlinearity increases from $\gamma^{(0)}$, the solutions only correspond to the low-transmission level until the transmission jumps to the high-transmission level. On the contrary, if we decrease the nonlinearity from the high-transmission state then we can find another stable solution. Thus this algorithm, called the continuation method, can be used to asses the optical bistability. Another advantage of the continuation method is that the number of iterations is much smaller if we compare with the weighted-averaged iterative method alone (34), see Fig. 2 (full-line).

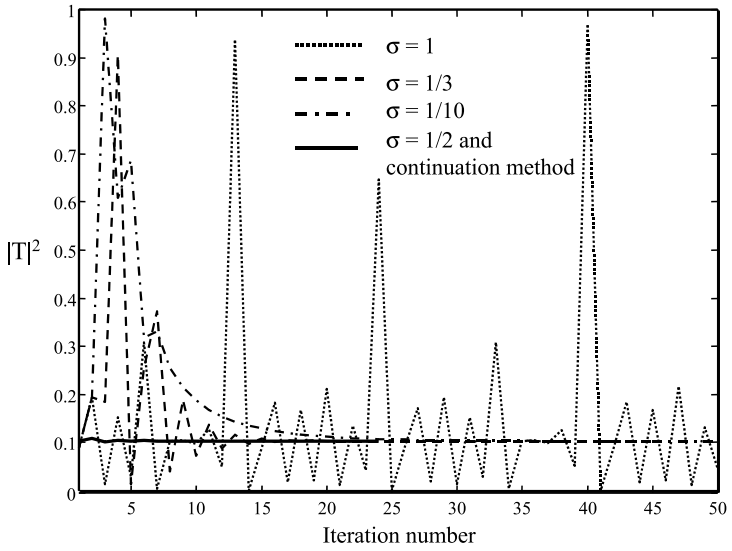

Figure 2: Transmissivity of a defect structure with $N = 10; \gamma_1 = 0$ and $\gamma_2 = 10^{-2}$ and $\widetilde{\omega} = 3.8483$ as a function of the iteration number for different values of σ. For $\sigma = 1/2$ the iteration does not converge and the result is not shown. However when we implement the combination between the weighted-averaged iterative method with $\sigma = 1/2$ and the continuation method, it produces a convergent solution with much smaller number of iteration.

4 Optical bistability in a finite periodic structure without and with defect

In this section we apply the numerical scheme that was derived in the previous section to study the transmission properties of structures as shown in Fig. 1. For both linear and nonlinear numerical calculations we take $n_1 = 1.125, n_2 = 2.25, w_1 = w_2 = \lambda_0/4$. The computational window of width $(1 + N/2)\,\lambda_0$ is divided into M equidistant elements with $h = \lambda_0/100$. All results given here have been found to be converged with respect to a refinement of the discretization and with respect to the iteration number. Before proceeding to the nonlinear case we first briefly discuss the linear structure by setting $\gamma = 0$. For the linear periodic or defect structures with $N = 10$, applying the improved FE scheme in place of the original one allows us to reduce the number of elements from about 2400 that are necessary to compute equally accurate results with scheme (19) to the number of 600 for the scheme (26). Within this accuracy, if we compare with the results of analytic transfer matrix, the improved FEM gave no observable differences on the scale of figures (3), (4) and (5). For the nonlinear structure, however, we do not have an exact analytical solution. Therefore we compared our numerical results with the results of the nonlinear transfer matrix method (Danckaert et al. 1991) using the full nonlinear interface conditions (Agarwal and Dutta Gupta ,1987). We remark that the nonlinear transfer matrix method is valid only for the case of weak nonlinearity. We observed a very good agreement between those two methods for the case of a defect structure but not for a perfect structure (for brevity, the data is not included in this paper). This can be understood from the fact that the maximum change of refractive index due to nonlinearity in an ideal structure is much bigger than that of a defect structure.

4.1 Transmission properties of the linear structure

It is well known that an infinite periodic structure has an essential property, i.e. the existence of forbidden bands prohibiting a certain range of frequencies of light waves to propagate through the structure. In other words, the electric field with frequencies inside the band gap are completely reflected by the

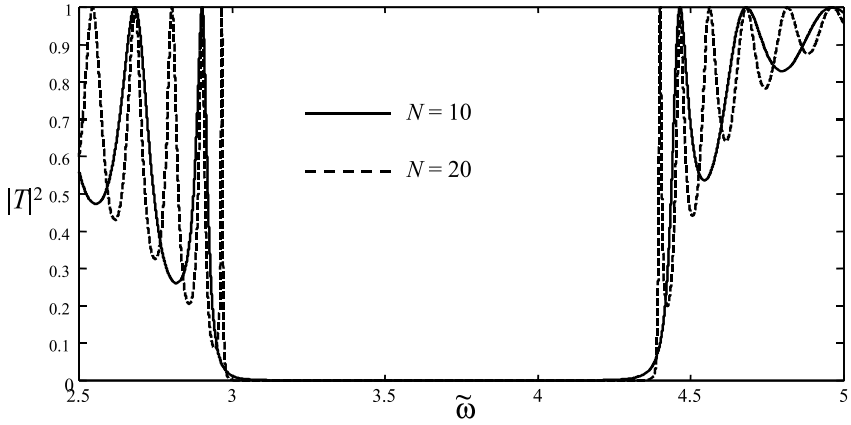

Figure 3: Transmission spectra of two periodic linear structures with $N = 10$ (solid) and $N = 20$ (dashed). The first band gaps of structures with $N = 10$ and $N = 20$ are respectively $\tilde{\omega} \in (2.9010, 4.4642)$ and $\tilde{\omega} \in (2.9673, 4.3996)$.

structure. However, in a finite periodic structure, the electric field in general will not be fully reflected. Consequently, the definition of band gap in a finite structure is questionable. According to common practice, in this paper we use the term band gap (of a finite structure) for the smallest frequency interval containing the band gap of the infinite structure that is bordered by two resonance frequencies (which are called band edge resonances). To get a feeling of this definition, we show in Fig. 3 the transmission spectrum around the first band gap of two linear finite gratings with 10 and 20 periods, respectively. As shown in this picture, the increasing number of periods reduces the length of the band gap. The reduction of the frequency band gap is saturated to the real band gap, i.e. the interval for an infinite periodic structure, which in this case is $\tilde{\omega} \in (2.9905, 4.3767)$. We notice that by adding more layers, the number of resonance frequencies where the transmission equals one is also increased and specifically the resonance at the band-edge becomes sharper. We also observe that for an N-period structure there are exactly N resonance frequencies at the left of the first gap confirming the analysis of Bendickson, Dowling and Scalora (1996).

When we introduce a defect layer in the middle of a finite periodic structure (see Fig. 1.b), a very narrow resonance that is isolated in the band gap occurs (see Fig. 4). The frequency of such a resonance is often called a defect mode frequency (see e.g. Busch, Chan and Soukoulis 1996 and Vasseur *et al.* 1999). This is in contrast with the case of a strictly periodic structure where all the resonances are concentrated at the border of the band gap (see Fig. 3). It is shown in Fig. 4.b that if we increase the number of periods and keep only one defect layer in the middle, more resonances outside the band gap appear and only one defect mode frequency inside the band gap exists. We found the defect modes for both $N = 10$ and $N = 20$ periods are approximately at the same frequency, i.e. at $\tilde{\omega} \approx 3.8599$. The isolated resonance for $N = 20$ is much thinner than that for $N = 10$; see the inset in Fig. 4.b. Furthermore, as can be seen in Fig. 5, the absolute value of the electric field inside the defect structure at the defect mode frequency is much larger than that of the periodic structure of the same length at the resonance frequency at the edge of the band gap. This electric field grows significantly when the number of periods is increased. Thus if a nonlinearity is included, the defect structure will enhance the nonlinear effect.

4.2 Bistable switching by frequency tuning

If a Kerr nonlinearity is introduced in the structure, it causes a change of the local refractive index and hence a change of the transmission spectrum. In general, a positive (negative) nonlinearity will shift nonlinearly the entire transmission spectrum to the left (right). Specifically when the resonance is sharp enough, bistability or multistability can be achieved (see. e.g. Agranovich *et al.* 1991). For

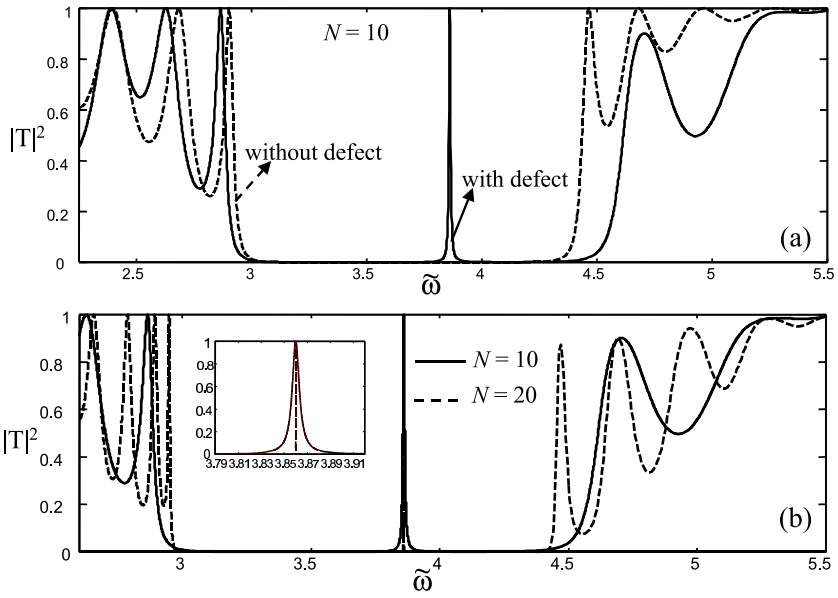

Figure 4: (a) Comparison between the transmission spectrum of a periodic structure (dashed-line) and that of a defect structure (full-line) with $N = 10$. The defect structure has a very narrow resonance which is isolated in the band gap. (b) Transmission spectra of a defect structure with $N = 10$ and $N = 20$, respectively. Observe that when the number of periods is increased, more resonances outside the band gap appear. The isolated resonance of the longer defect structure is much thinner than that of the shorter one, see inset.

a strictly periodic structure, bistability usually occurs around the resonance peak at the border of the linear band gap: a positive (negative) nonlinearity effects bistability in the left (right) flanks of the resonance frequencies. For example we show in Fig. 6 the transmission spectra of the nonlinear periodic structures (γ positive) for $N = 10$ and $N = 20$ respectively in the vicinity of the resonance peak at the top of the first linear band gap. Each spectrum is calculated using a fixed nonlinearity γ. For a certain threshold of γ, the spectrum exhibits a bistability phenomenon: by increasing the frequency of a tunable source, the transmission jumps into high-transmission state $1'$ after it passes point 1. Similarly, the low-transmission state $2'$ can be reached after passing state 2 when moving in the opposite direction, see Fig. 6.a. For $N = 10$ bistability can be obtained when we set $\gamma_2 = 0.05$ in all high index layers but not when $\gamma_2 = 0.025$. When the number of layers is doubled such that $N = 20$, the transmission spectrum already exhibits bistability for $\gamma_2 = 4 \times 10^{-3}$. Adding γ not only in the high index layers but also in the low index layers can reduce the threshold for bistability, further see Fig. 6.b.

For a nonlinear defect structure the bistability can occur in the vicinity of the resonance peak at the bottom of the linear band gap or around the defect mode frequency where the resonance is relatively sharp. As we notice before the electric field intensity inside the defect structure at the defect mode frequency is very high so that we can use it to enhance the nonlinear effect. Therefore bistable behavior can be expected around this frequency with a lower threshold compared with a periodic structure of the same length. And indeed this case is confirmed by our numerical calculations. Figure 7 shows the transmission spectra of the nonlinear defect structure with $N = 10$ for different γ's. The bistability can already be observed for $\gamma = 5 \times 10^{-4}$ and $\gamma = 4 \times 10^{-4}$ for the cases where nonlinearity is added in the high index layers only and in both high and low index layers, respectively.

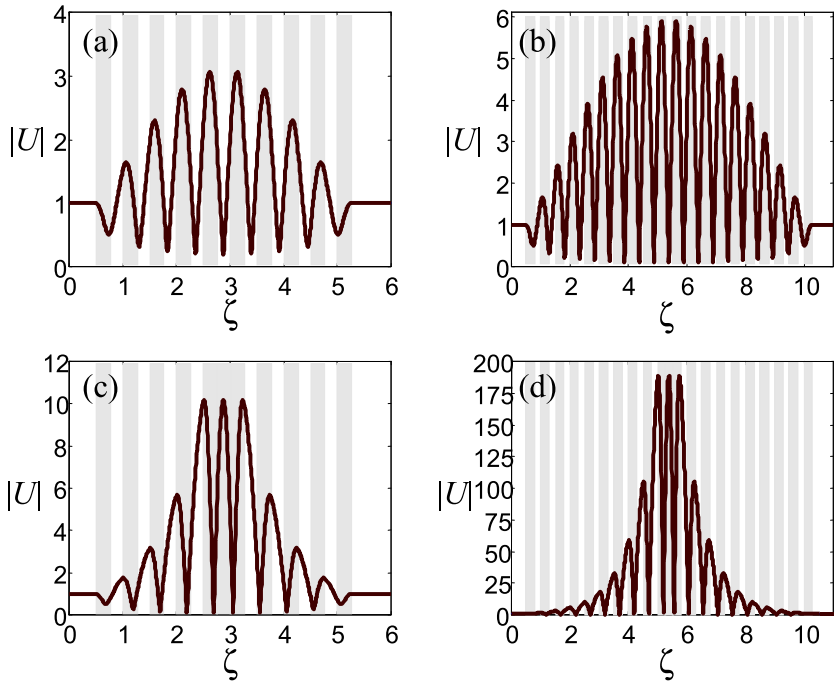

Figure 5: The normalized absolute value of the electric field inside (a) a periodic structure, $N = 10$; (b) a periodic structure, $N = 20$; (c) a defect structure, $N = 10$; (d) a defect structure, $N = 20$. All plots correspond to linear resonant configurations with full transmission. The frequencies (a) $\widetilde{\omega} = 2.9019$ and (b) $\widetilde{\omega} = 2.9673$ are at the band-edge, and the defect mode frequencies are (c) $\widetilde{\omega} = 3.8599$ and (d) $\widetilde{\omega} = 3.8599$. The amplitudes on the input and output segments are equal to one. Observe that the maximum value of $|U|$ of the defect structure is much larger than than of the periodic structure with the same length.

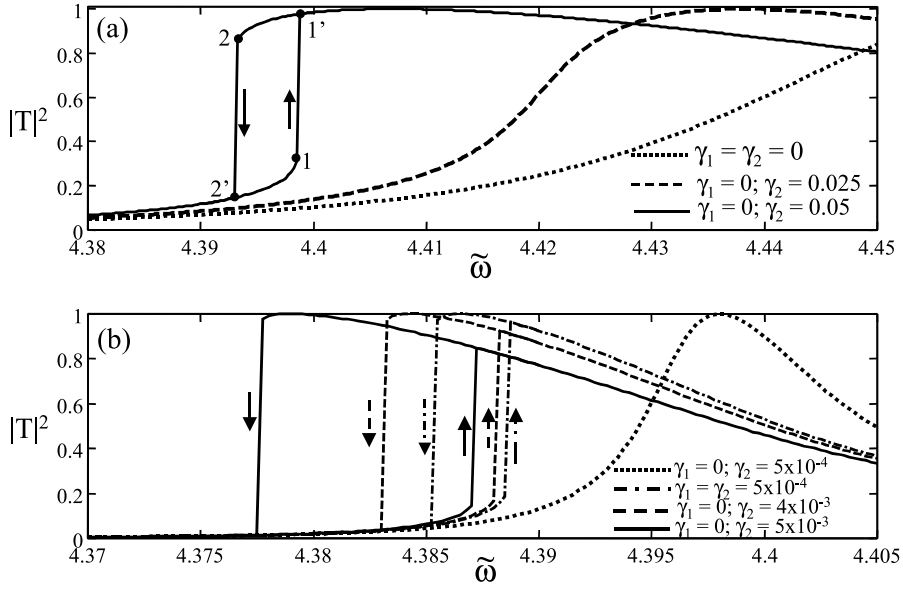

Figure 6: Transmission spectra of two nonlinear periodic structures with (a) $N = 10$ and (b) $N = 20$. Observe that for a certain threshold γ, a periodic structure can exhibit a bistable switching.

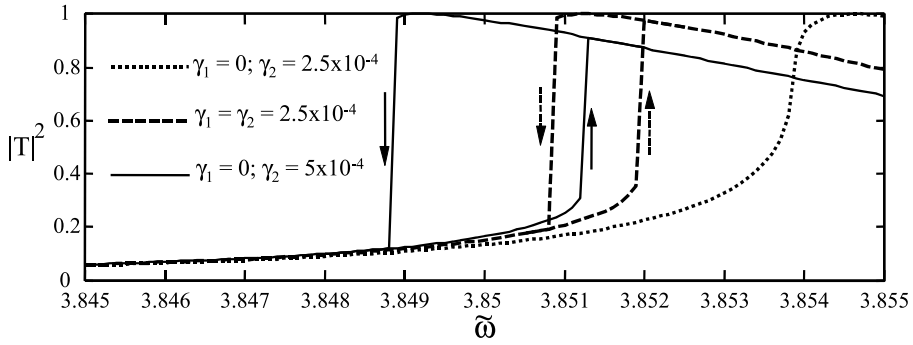

Figure 7: Transmission spectra of a nonlinear periodic structure with defect and $N = 10$. The threshold for bistability of a defect structure is much lower than that of a periodic structure with the same length.

4.3 Bistability controlled by input intensity

The discussion in the previous section suggests the possibility for the use of a finite (defect) periodic structure as a device in which bistable switching is controlled by frequency tuning while input electric field is maintained at fixed power. As can be seen in Fig. 6, we observe that for a certain frequency, e.g. $\widetilde{\omega} \approx 4.375$, the transmissivity is found uniquely for relatively low γ, then it is multiple-valued for larger γ. However, by increasing the value of γ the transmissivity can be unique again. This fact also shows the possibility of optical bistability controlled by input light intensity with fixed frequency (we have noticed in Sec. 2 that γ can also be considered as the input intensity).

In Fig. 8 we present the input-output characteristics of a finite periodic structure when the frequency is chosen close to the resonance peak at the top of the first linear band gap. Notice that the resonance frequencies for $N = 10$ and $N = 20$ are respectively $\widetilde{\omega} \approx 4.4642$ and $\widetilde{\omega} \approx 4.3996$. Bistable behavior can not be obtained when the input field has a frequency that is relatively close to the resonance frequency, e.g. in the case of $\widetilde{\omega} = 4.410$ for $N = 10$ and $\widetilde{\omega} = 4.395$ for $N = 20$. If a smaller frequency is chosen, bistability is observed; however the smaller frequency (farther from the resonance frequency) will increase the threshold of γ: e.g. for $N = 10$, the threshold of ~ 0.048 for $\widetilde{\omega} = 4.400$ is increased to ~ 0.056 if $\widetilde{\omega} = 4.395$ is used. The same phenomenon also holds for the case of a longer grating. Furthermore, as in the case of bistability tuned by frequency, the upswitching threshold can be reduced by increasing the number of layers. Indeed the bistable behavior in a periodic structure with $N = 20$ is already achieved with upswitching threshold $\gamma_2 \approx 0.0026$ for $\widetilde{\omega} = 4.39$. We also remark that the threshold of bistability can also be decreased by introducing the nonlinearity not only in the high index layers but also in the low index layers (the results of these calculation are not presented here).

A defect layer that is located in the middle of a periodic structure can also be used to reduce the threshold of bistability. In order to realize it, $\widetilde{\omega}$ should be tuned to a value close to the linear defect mode frequency. In Fig. 9 we plot the transmissivity of a nonlinear defect structure with $N = 10$ as function of input power γ. We show in Fig. 9.a. the case when the nonlinearity is only introduced in all high index layers for three different frequencies. For a frequency that is too close to the defect mode the bistability cannot be achieved. When the frequency is farther from the defect mode, the upswitching threshold is increased. In Fig. 9.b. we fix the frequency at $\widetilde{\omega} = 3.85$ and compare three different cases, i.e. when the nonlinearity is introduced (1) only in defect layer, (2) only in high index layers and (3) in both high and low index layers. The thresholds value γ for cases (1), (2) and (3) are approximately $1.6 \times 10^{-3}, 6.85 \times 10^{-4}$ and 4.12×10^{-4}, respectively. In general these threshold value are much smaller than that of a nonlinear strictly periodic structure of the same length.

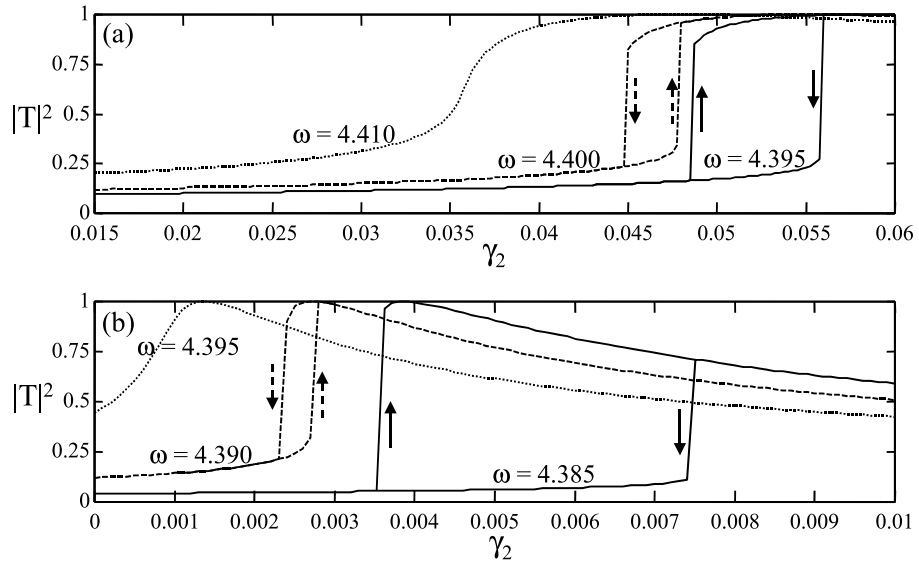

Figure 8: Input-output characteristics of a finite periodic structure for (a) $N = 10$ and (b) $N = 20$ periods versus the input light intensity where the nonlinearity is only introduced in the high refractive index layers. The threshold for bistability decreases as the number of periods is increased.

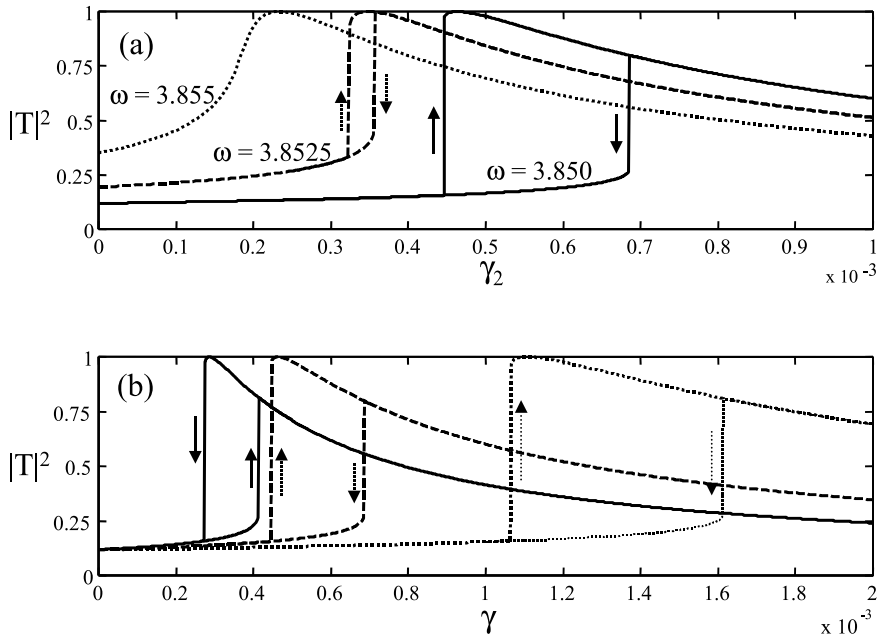

Figure 9: Input-output characteristics of a defect structure for $N = 10$. (a) The nonlinearity is introduced in all high index layers with normalized frequency 3.8500, 3.8525 and 3.8550; respectively. (b) The normalized frequency is set to be 3.85 and the nonlinearity is introduced only in defect layer (dotted-line); in all high index layers (dashed-line); and in all high and low index layers (full-line).

5 Conclusions

A numerical scheme to study the nonlinear optical response of a one-dimensional finite grating has been presented. It directly implements the one-dimensional nonlinear Helmholtz equation and exact transparent-influx boundary conditions without introducing any approximation except the finite element discretization. For the present configurations with piecewise constant refractive index and nonlinearity, even the integrations of the projected functional of the NLH in the finite element space can be calculated explicitly. This is different from the nonlinear transfer matrix formalisms mentioned in Sec. 1 that are based on the SVEA and other approximations. Therefore, our method can be used to study the validity of those approximative methods.

When compared to the usual second order FEM approach, the scheme with fourth order correction as proposed in this paper provides a significant improvement in term of computational effort for linear problem.

While our analysis focuses on layer stacks with step-like refractive indices, the presented method can be applied easily to more general structures, i.e. not necessarily periodic nonlinear gradient or piecewise constant permittivity profiles.

References

[1] Agarwal, G.S., and S. Dutta Gupta, *Opt. Lett.* 12(10), p. 829-831, 1987.

[2] Agranovich, V.M., S.A. Kiselev, and D.L. Mills, *Phys. Rev. B* 44(19), p. 10917-10920, 1991.

[3] Atkinson, K.E., *An introduction to numerical analysis*, 2nd edn, John Wiley & Sons, Inc., New York, 1989.

[4] Bayindir, M., C. Kural, and E. Ozbay, *J. Opt. A: Pure Appl. Opt.* 3, p. S184-S189, 2001.

[5] Bendickson, J.M., J.P. Dowling, and M. Scalora, *Phys. Rev. E.* 53(4), p. 4107-4121, 1996.

[6] Busch, K., C.T. Chan, and C.M. Soukoulis, in Ref. [19], p. 465-485, 1996.

[7] Chen, W. and D.L. Mills, *Phys. Rev. B 35(2)*, p. 524-532, 1987a.

[8] Chen, W. and D.L. Mills, *Phys. Rev. B 36(12)*, p. 6269-6278, 1987b.

[9] Danckaert, J., H. Thienpont, I. Veretennicoff, M. Haelterman, and P. Mandel, *Opt. Comm.* 71(5), p. 317-322, 1989.

[10] Danckaert, J., K. Fobelets, and I. Veretennicoff, *Phys. Rev. B* 44(15), p. 8214-8225, 1991.

[11] Dutta Gupta, S. and G.S. Agarwal, *J. Opt. Soc. Am. B* 4(5), p. 691-695, 1987.

[12] He, J. and M. Cada, *Appl. Phys. Lett.* 61(18), p. 2150-2152, 1992.

[13] He, G.S. and S.H. Liu, *Physics of Nonlinear Optics*, World Scientific, Singapore, 1999.

[14] Kasyap, R., *Fiber Bragg Gratings,* Academic Press, San Diego, 1999.

[15] Lidorikis, E., K. Busch, Q.M. Li, C.T. Chan, and C.M. Soukoulis, *Phys. Rev. B* 56(23), p. 15090-1599, 1997.

[16] Lu, X., Y. Bai, S. Li and T. Chen, *Opt. Comm.* 156, p. 219-226, 1998.

[17] Marburger, J.H. and F.S. Felber, *Phys. Rev. A* 17, p. 335-342, 1978

[18] Soukoulis, C.M. (ed.), *Photonic Band Gaps and Localization*, Plenum, New York, 1993.

[19] Soukoulis, C.M. (ed.), *Photonic band gap materials*, Kluwer Academic, Dordrecht, 1996.

[20] Tran, P., Opt. Lett. 21(15), p. 1138-1140, 1996.

[21] Tran, P., *J. Opt. Soc. Am. B* 14(10), p. 2589-2595, 1997.

[22] Vasseur, J.O., B. Djafari-Rouhani, L. Dobrzynski, A. Akjouj, and J. Zemmouri, *Phys. Rev.* B 59(20), p. 13446-13452, 1999.

[23] Wang, R., J. Dong and D.Y. Xing, *Phys. Rev. E* 55(5), p. 6301-6304, 1997.

[24] Winful, H.G., J.H. Marburger and E. Garmire, *Appl. Phys. Lett.* 35(5), p. 379-381, 1979.